Molecular and solid-state properties of tris-(8-hydroxyquinolate)-aluminum

Richard L. Martin and Joel D. Kress
Theoretical Division, MS B268, Los Alamos National Laboratory, Los Alamos, New Mexico 87545

I. H. Campbell and D. L. Smith
Materials Science and Technology Division, MS D429, Los Alamos National Laboratory, Los Alamos, New Mexico 87545
(Received 22 December 1999)

We use a hybrid density-functional-theory approach to calculate ground-state electronic properties and a time-dependent density-functional-theory approach to investigate the excited state electronic properties of molecular tris-(8-hydroxyquinolate)-aluminum, Alq. The calculated molecular results are compared with measurements on dense solid-state films of Alq. We specifically consider: the optical absorption spectrum near the fundamental absorption threshold, the ionization potential, the single-particle energy gap, the static dielectric constant, and the electric-field dependence of the electron mobility. We find that the molecular calculations can describe the optical absorption spectrum near the fundamental absorption threshold without significant corrections for solid-state effects. The energies of the triplet excited states are computed and the lowest triplet is found to lie 0.64 eV below the lowest excited singlet state. In contrast, large dielectric corrections must be included for the molecular calculations to describe the ionization potential and single-particle energy gap. When these dielectric corrections are made, using the calculated molecular polarizability, which accurately gives the measured static dielectric constant, both the ionization potential and single-particle energy gap are well described. The calculated molecular dipole moment can be used to interpret the electric-field dependence of the electron mobility. The solid-state properties, determined from the molecular calculations, are then used in a device model to describe the measured current-voltage characteristics in Alq diodes.

I. INTRODUCTION

Conjugated organic materials are now used as the emissive layer in organic light-emitting diodes and they are also being investigated for a large variety of other electronic applications. It is of both scientific interest and technological importance to be able to predict the properties of dense solid-state films based on the properties of the isolated, constituent organic molecules. It is particularly desirable to be able to predict the solid-state electronic properties using calculated molecular properties since this would enable rational design of individual molecules for device applications. The general goal is to be able to use calculated molecular properties to predict solid-state film properties and then incorporate these solid-state properties into a device model to predict device behavior.

Two important organic electronic devices are light-emitting diodes and field-effect transistors. For these devices critical solid-state properties include the solid-state ionization potential (IP_s), the solid-state electron affinity (EA_s), the single-particle energy gap ($E_g = IP_s - EA_s$), and the charge-carrier mobilities and optical properties near the absorption threshold. The single-particle energy gap, IP_s and EA_s largely determine the charge injection properties of metal electrodes in contact with the organic material and the carrier mobilities determine the current in the device for a given charge density and electric field. The optical properties near the absorption threshold are important for light-emitting diodes. Tris-(8-hydroxyquinolate)-aluminum, Alq, has been widely studied because of its use in light-emitting diodes.[1] Films of Alq are used as both light emitting and as electron-transport layers. Although Alq is typically used in multiple organic layer device structures it has recently been studied in single layer structures where the properties of thin Alq films can be measured more directly.[2]

In this paper, we use a hybrid density-functional theory (DFT) to calculate ground-state electronic properties and time-dependent density-functional theory (TDDFT) to investigate the excited-state electronic properties of molecular Alq. The calculated molecular results are compared with measurements on dense solid-state films of Alq. We wish to determine which calculated properties of the isolated molecules can be used directly to interpret the results of measurements on dense solid-state films and which calculated molecular properties must be corrected for solid-state effects to describe the electronic properties of these films. We find that the optical properties near the absorption threshold of the solid-state film are well described by the molecular calculations without modification. The optical transitions in this energy range are from the ground state to a molecularly localized neutral excited state. The states involved are not strongly perturbed in the condensed phase. By contrast we find that properties that involve energies of electrically charged states such as the ionization potential and the single-particle energy gap, cannot be directly described by the molecular calculations. However, if polarization corrections, which are rather large, are included, the molecular calculations can then describe these charged state properties. We find that the calculated molecular polarizability accurately describes the solid-state polarization corrections and can be used to determine the measured static dielectric constant. The calculated molecular dipole moment can be used to interpret the electric-field dependence of the electron mobility. The solid-state properties, determined from the molecular calculations, are then used in a device model to describe the measured current-voltage characteristics in Alq diodes.

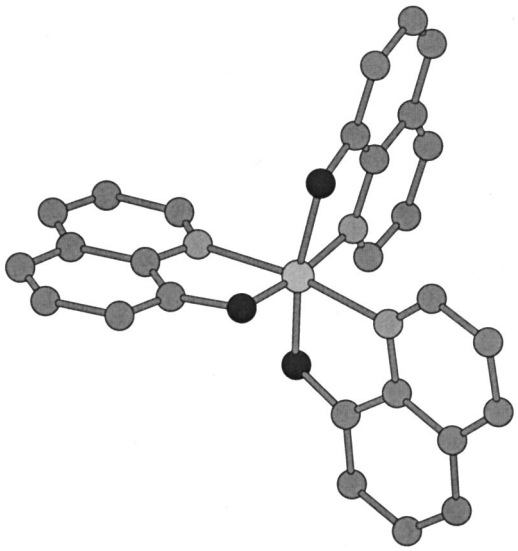

FIG. 1. The meridianal isomer of Alq. The darker cirlces about the central Al represent oxygen atoms. Hydrogens bound to the ring carbons are not shown.

The paper is organized as follows: in Sec. II, we present the results of the molecular calculations; in Sec. III, we present the results of measurements on dense solid-state films of Alq and compare these results with the molecular calculations; and in Sec. IV we state our conclusions.

II. MOLECULAR CALCULATIONS

An individual Alq molecule consists of a central aluminum atom coordinated by three quinolate ligands, each of which binds to the metal site via oxygen and nitrogen donors, thereby giving a pseudo-octahedral environment for the aluminum. There are two isomers with different chirality; the meridianal isomer shown in Fig. 1 and the facial isomer shown in Fig. 2. The meridianal isomer is more stable and is generally the major constituent of thin films.

Despite its technological importance, there are relatively few theoretical studies of the electronic structure of Alq.

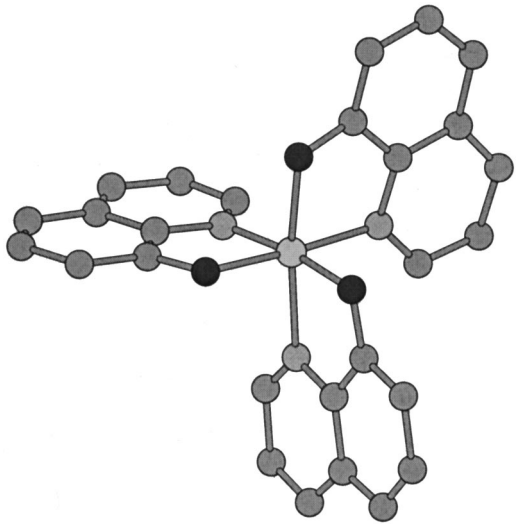

FIG. 2. The facial isomer of Alq. This isomer is computed to be slightly less stable (~ 5 kcal/mol) than the meridianal form.

Semiempirical ZINDO (Ref. 3) calculations by Burrows *et al.*[4] provided the first qualitative overview of the electronic structure. The optical transition to the lowest excited singlet state was found to correspond to an excitation of an electron from an orbital with amplitude primarily on the oxygen side of the quinolate to one with amplitude largely on the nitrogen side. Combinations of these excitations on the three ligands give rise to three low-lying, nearly degenerate excited singlets.

Very recently, density-functional theory calculations on this material using a generalized-gradient approximation (GGA) were reported by Curioni *et al.*[5–7] This work provided a detailed description of structural features and geometrical relaxation processes accompanying charge injection in molecular Alq. The excited-state spectrum was generated within a one-electron approximation in which the character of particle-hole excited states was inferred from the convolution of the eigenvalue spectra of individual electrons and holes. The nature of the low-lying states agreed well with the earlier assignments, although the absolute excitation energies implied significant ''excitonic'' corrections.

Here, we utilize a hybrid DFT method, B3LYP.[8] It is primarily distinguished from the GGA used by Curioni *et al.* by the presence of a component of the full, nonlocal Hartree-Fock exchange term. This approach often gives improved bond energies and geometries in organic molecules compared with the GGA's. However, we find that in all cases where we can compare, our results are in excellent agreement with those of Curioni *et al.* For example, we find the meridianal isomer to be ~ 5 kcal/mol more stable than the facial form. Curioni *et al.* found the same ordering with an energy difference of ~ 4 kcal/mole. Their estimate also includes zero-point corrections, which are found to be quite small (0.4 kcal/mol favoring the facial form). The qualitative nature of the bonding, the eigenvalue patterns, the charge densities, and the nature of the lowest excited states are also in good agreement with the DFT results of Curioni *et al.* Here we concentrate on properties that are directly related to solid-state electronic properties of Alq with which we will compare.

The geometries of both isomers were optimized using the hybrid B3LYP approximation, a 6-31G* basis set, and the Gaussian suite of programs.[9] Selected geometrical parameters describing the two isomers at their respective minima are given in Table I. The meridianal form has been characterized experimentally, and the Al-O distances range from 1.85–1.86 Å in one determination and 1.84–1.88 Å in another.[10,11] These compare favorably with the 1.86–1.89 Å range from the B3LYP calculation. The Al-N distances of 2.06–2.13 Å are only slightly longer than the experimental determination 2.03–2.08 Å.[10,11] It is interesting to note that the commonly used semiempirical approximations, AM1 and PM3, both yield disappointing geometries for Alq. The Al–N distance, in particular, is in error on the order of 0.3–0.4 Å.[5]

The dipole moments d of both isomers are large. In the meridianal isomer, the dipole is oriented toward the oxygen atom, which has a nitrogen trans to it (i.e., the oxygen pointing towards the reader in Fig. 1). In the facial isomer (Fig. 2), it points to the center of the triangular face defined by the three oxygens coming towards the reader. The molecular

TABLE I. Properties computed for Alq. The units are Å for distances, Debye for dipole moments d, atomic units for the static polarizability $\bar{\alpha}$, and eV for the vertical molecular ionization potentials (IP_m) and electron affinities (EA_m). The B3LYP calculations used the 6-31G* basis set, with the exception of the electron affinites and ionization potentials, which were computed with the 6-31+G* basis set. The latter contains the diffuse functions necessary to describe the negative ion, and hence the electron affinity. By way of comparison, the calculations of Curioni *et al.* give (for the meridianal isomer) $d=4.1$ D, $IP_m=6.15$ eV, and $EA_m=0.95$ eV.

Property	B3LYP
Meridianal	
R_{AlO}	1.86,1.89,1.88
R_{AlN}	2.08,2.13,2.06
d	5.3
$\bar{\alpha}$	327
IP_m	6.60
EA_m	0.83
Facial	
R_{AlO}	1.85
R_{AlN}	2.13
d	7.9
$\bar{\alpha}$	330
IP_m	6.65
EA_m	0.85

ionization potential (IP_m) and electron affinity (EA_m) reported in Table I are for vertical transitions in which the molecular geometry of the ground state is used for the ions. For the meridianal isomer, we find structural relaxation energies of 0.09 eV for the positive ion and 0.11 eV for the negative ion, similar to the values of 0.04 eV and 0.06 eV computed by Curioni *et al.*[5] The static polarizability $\bar{\alpha}$ is found to be reasonably isotropic, as might be expected for a pseudo-octahedral species, and very similar in both isomers.

We have studied the excited-state spectrum of the isolated molecule with time-dependent density-functional theory.[12–15] This technique is effectively the random-phase approximation applied within DFT. Recent implementations of the method by Bauernschmitt and Ahlrichs[16] and Stratmann *et al.*,[17] compared the performance of a variety of functionals for a set of organic molecules. Both groups found that TDDFT was surprisingly accurate and that the hybrid functionals gave slightly more accurate excitation energies than GGA's, although they pointed out that an intensive study has yet to be performed.

Table II reports the vertical excitation energies and oscillator strengths (length form) for the first ten excited singlet states of the meridianal form of Alq. The qualitative nature of the lowest excited singlets in the TDDFT calculations is compatible with that found in the earlier semiempirical work.[4] In each isolated ligand the highest occupied molecular orbital is located principally on the phenoxide side of the ring and the lowest unoccupied molecular orbital principally on the nitrogen side. In the complex, linear combinations of these give rise to three high-lying occupied orbitals and three low-lying virtuals. The first nine excited states of Table II correspond to excitations among the three phenoxidelike occupied orbitals to the three pyridyl-like orbitals.

TABLE II. Singlet and triplet vertical excitation energies for the meridianal isomer of Alq in the TDDFT approximation using the B3LYP functional and the 6-31G* basis set. For singlets, the oscillator strength computed in the length form is given parenthetically.

Root	$\Delta E(S=0)$	$\Delta E(S=1)$
1	2.77(0.006)	2.13
2	2.90(0.068)	2.16
3	2.94(0.001)	2.19
4	2.97(0.042)	2.79
5	3.03(0.001)	2.95
6	3.15(0.014)	3.06
7	3.26(0.003)	3.23
8	3.27(0.006)	3.24
9	3.35(0.003)	3.31
10	3.97(0.011)	3.35

The lowest triplet state in the TDDFT calculations is predicted to occur at 2.13 eV, 0.64 eV below the lowest singlet state. It involves an orbital excitation analogous to the lowest singlet. It is also possible to perform direct spin-unrestricted Kohn–Sham calculations on the lowest triplet. At the optimized ground-state geometry, this approach gives the lowest triplet 2.39 eV above the ground state, only slightly larger than the TDDFT result. We examined the magnitude of geometry relaxation in the triplet and found that it is stabilized by 0.39 eV.

III. COMPARISON WITH MEASURED SOLID-STATE PROPERTIES

The solid-state properties of Alq thin films were determined using a variety of Alq test structures. Optical absorption measurements were made on thin (100 nm) films of Alq deposited on quartz substrates. Structures for electrical measurements consisted of a thin (10 nm), semitransparent metal on a glass substrate, an Alq layer 50–2000 nm thick, and a top, thick (100 nm) metal contact. The semitransparent contact was deposited either by sputter deposition (Cu, Au, Pt) or resistive evaporation (Ca, Mg, Sm, Al). The Alq and top metal contacts were resistively evaporated in a cryo-pumped vacuum system with a base pressure of 2×10^{-8} Torr. The structures were fabricated and tested in an inert atmosphere at room temperature. Capacitance-voltage measurements were used to measure the film dielectric constant and to verify that the metal/Alq/metal structures were fully depleted.

The optical absorption spectrum of a thin solid film of Alq is shown in Fig. 3. For comparison, graphical representations of the TDDFT calculated singlet excitation energies and oscillator strengths from Table II are also shown in Fig. 3. Overall, the agreement between calculation and experiment is very good for the low-energy transitions. The onset of absorption is predicted at 2.77 eV, in close agreement with the observed onset. The most intense transitions, from states 2 and 4, are underestimated by a few tenths of an eV. Above $\sim$3.5 eV, the agreement with experiment is not as satisfactory. This may be a basis set artifact. The excited-state cal-

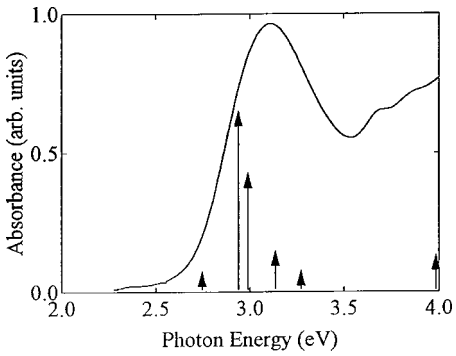

FIG. 3. The absorption spectrum of Alq. The vertical lines represent the energies and oscillator strengths predicted by the time-dependent DFT calculations described in the text.

culations use the 6-31G* basis, which is expected to be adequate for the ground state and first few excited states. It is deficient, however, in lacking the diffuse functions needed to describe Rydberg character in the excited states. At present, inclusion of such diffuse functions requires excessive computation time. This basis set deficiency is expected to become more severe at higher energies. The missing spectral intensity in the region from 3.5–4.0 eV is likely due more to this omission than to a failure of either the functional or the basic approximations of TDDFT. Solid-state effects could have a greater impact on the high-energy transitions than on the transitions near the absorption edge. Although there may be some difficulty with the higher-energy transitions, absorption near the fundamental absorption edge in the dense solid-state film is well described by the molecular calculations. The measured dielectric constant of thin films of Alq is 3.0 ± 0.3 as determined from the capacitance of device structures. The dielectric constant of the Alq thin films can be calculated from the molecular polarizability and the Clausius–Mossotti relation. The dielectric constant is

$$\epsilon = \frac{3+2\chi\bar{\alpha}}{3-\chi\bar{\alpha}}, \tag{1}$$

where $\bar{\alpha}$ is the static polarizability, $\chi = 4\pi N$, and N is the density of molecules in the solid. Using the molecular polarizability for the meridianal structure $\bar{\alpha} = 327$ a.u. and a molecular density (taken from the crystal structure) of $N = 2.0 \times 10^{21}$ molecules/cm^3, the calculated dielectric constant is 3.0, in excellent agreement with the experimental value.

The single-particle energy gap of dense organic materials is an important parameter for organic electronic devices. It is not sufficient to measure the optical absorption spectrum to determine this quantity because there can be significant excitonic effects that are difficult to estimate reliably. In principle, the single-particle energy gap can be measured using a combination of photoemission and inverse photoemission but it has proven difficult to obtain adequate signals from thin, insulating organic films. We have determined the single-particle energy gap of Alq using a combination of internal photoemission and built-in potential measurements in device structures.[2] Internal photoemission and built-in potential measurements determine the relative energy position of various contact metals with respect to the electron and hole polaron levels of the Alq thin film. Figure 4 shows the

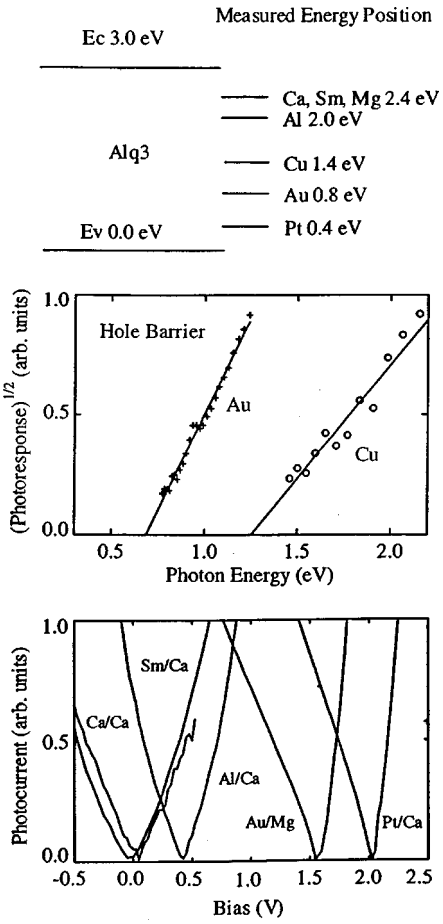

FIG. 4. Electron energy diagram for metal contacts to Alq derived from internal photoemission and built-in potential measurements (top). Internal photoemission measurements of the hole energy barrier for Au and Cu contacts to Alq (middle). Magnitude of the photocurrent as a function of bias voltage between the anode/cathode (bottom). The photocurrent is nulled when the applied bias cancels the built-in potential.

measured energy level diagram for various metals in contact with Alq (top) and representative internal photoemission (middle) and photocurrent vs bias (bottom) measurement results used to determine these energy levels.

In the internal photoemission technique,[18] photons are absorbed in a thin metal contact producing hot electrons and holes. The hot electrons (or holes) give rise to a photocurrent as they move from the metal into the organic film. The photocurrent yield is

$$\text{yield} \propto (h\nu - \phi)^2, \tag{2}$$

where $h\nu$ is the photon energy and ϕ is the energy barrier between the metal Fermi level and the conduction (E_c) or valence (E_v) levels of the Alq film. The energy barrier is measured by extrapolating the square root of the photocurrent yield as shown in Fig. 4. The extrapolated energy barrier is about 0.7 eV for Au and about 1.3 eV for Cu. These extrapolated barriers are not the zero electric-field energy barriers. There is an electric field in the Alq film and an image charge potential in the metal when the electron is emitted into the organic. This effect lowers the extrapolated threshold in the films by about 0.1 eV for the experimental

conditions used. The zero-field energy barriers are thus the extrapolated thresholds plus the correction for the image potential.

Measurements of the photocurrent as a function of bias can be used to determine the differences between the metal contact energy levels. At zero bias in a fully depleted metal/organic/metal structure, there is a built-in potential equal to the difference between the metal contact energy levels. The photocurrent is proportional to the electric field in the structure, which can be nulled by application of an external dc bias. The results shown in Fig. 4 were made using modulated, above energy gap light and phase-sensitive detection. The built-in potential in the structure is the bias at which the photocurrent is minimum. The built-in potential is near zero for Ca/Ca and Sm/Ca, about 0.4 V for Al/Ca, about 1.6 V for Au/Mg, and about 2 V for Pt/Ca. The built-in potential of 2 V for Pt/Ca structures means that the Fermi-level difference between Pt and Ca electrodes is 2 eV.

By combining internal photoemission and photocurrent vs bias results, the single-particle energy gap, i.e., the separation between the conduction and valence levels of the film, can be determined. The single-particle energy gap of Alq determined using these techniques is 3.0 eV$\pm$0.2 eV as indicated in Fig. 4. These techniques measure the differences between the metal Fermi energies and the electron and hole polaron levels of the Alq film. They do not provide a direct measurement of these energy levels with respect to vacuum.

The experimental solid-state ionization potential is 5.6–6.0 eV,[19] which is nearly 1 eV smaller than the calculated molecular ionization potential and the measured solid-state single-particle energy gap is more than 2 eV smaller than the computed difference between the molecular ionization potential and electron affinity ($IP_m - EA_m \sim 5.8$ eV). These discrepancies come about from the additional stabilization associated with the charged states in the solid-state film due to polarization of the neighboring molecules and from vibronic relaxation.[20] The polarization stabilizes both the positive ion, thereby decreasing the ionization potential of the solid, and the negative ion, thereby increasing the electron affinity, relative to what would be measured or computed for the isolated molecule. Such polarization corrections are much less important for the neutral excited states, which appear in optical property calculations because the response of the environment to a local dipole is much less than that for a charge.

The solid-state ionization potential and single-particle energy gap of the Alq film can be calculated using the theoretical electron affinity and ionization potential of the molecule and correcting for solid-state polarization effects and vibronic relaxation. We assume the permanent dipole moments of the various Alq molecules are oriented so that their interaction energy with the localized charge cancels, and on average, makes no net contribution to the stabilization energy. This interaction of the charge with the permanent dipole moments leads to an inhomogeneous broadening, but not a net shift, of the energy distribution because of disorder in the neighboring dipole orientation at various molecular sites. The induced dipoles are oriented by the localized charge and are all directed toward (or away) the charge and have same sign energy contribution. The stabilization energy due to interaction with the induced dipoles is[21]

$$E_{\text{polar}} = \sum_i \frac{1}{2} \vec{d}_i \frac{e\hat{r}_i}{r_i^2} \quad , \tag{3}$$

where $\vec{d}_i$ is the induced dipole moment at molecule i and r_i the intermolecular distance. To estimate this induced polarization correction we enclose the charged Alq molecule of interest in a spherical cavity also containing the ten nearest Alq molecules in the x-ray crystal structure.[22] The radius of this cavity is $r_0 = 1.1$ nm. The polarization energy from the ten near-neighbor molecules is calculated directly. This energy is then augmented using a continuum approximation and the Clausius-Mossotti relation for the more distant Alq molecules.[21] Our estimate of the stabilization energy is then

$$E_{\text{polar}} = \sum_i \frac{1}{2} \frac{\bar{\alpha} e^2}{r_i^4} + \frac{1}{2} \frac{(\epsilon - 1) e^2}{\epsilon r_o}, \tag{4}$$

where the sum is over the ten near neighbor molecules and the second term on the right is the contribution from the more distant molecules . The solid-state ionization potential and single-particle energy gap are then

$$\text{IP}_s = \text{IP}_m - E_{\text{polar}} - E_{vib(h)}, \tag{5}$$

$$E_g = (\text{IP}_m - \text{EA}_m) - 2E_{\text{polar}} - E_{vib(e)} - E_{vib(h)}, \tag{6}$$

where $E_{vib(e,h)}$ is the vibronic relaxation energy for the electron (hole) polaron. The sum over the ten nearest molecules gives a stabilization energy of 0.70 eV. With $r_0 = 1.1$ nm and $\epsilon = 3.0$, the continuum correction is 0.44 eV. The total polarization correction is thus 0.70 eV+0.44 eV $=$1.14 eV. The calculated vibronic relaxation for the hole polaron is 0.09 eV. The solid-state ionization potential is then 6.60 eV$-$1.14 eV$-$0.09 eV$=$5.37 eV, which is in reasonable agreement with the experimental values that range from 5.6–6.0 eV. The sum of the calculated vibronic relaxation energies (for electron and hole) is 0.20 eV. The energy gap is then 6.60 eV$-$0.83 eV$-$(2$\times$1.14 eV) $-$0.2 eV$=$3.29 eV. This is in reasonable agreement with the experimental result of 3.0 eV$\pm$0.2 eV presented above. Thus the molecular calculations give good agreement for the solid-state ionization potential and single-particle energy gap after polarization corrections and the vibronic relaxation energy is included.

The transport properties of electrons in Alq thin films were measured using the time-of-flight technique. In this technique, a semitransparent blocking contact/film/blocking contact structure is used. An optical pulse incident on the material through the semitransparent contact, creates a thin sheet of electron-hole pairs next to the contact and, depending upon the sign of the applied bias, electrons or holes are driven across the sample. The absorption depth of the optical excitation is small compared to the film thickness and the optical pulse duration is short compared to the transit time of the charge carriers across the sample. Low-intensity optical pulses are used so that the photogenerated charge-carrier density does not significantly perturb the spatially uniform electric field in the structure. The carrier mobility μ is given by

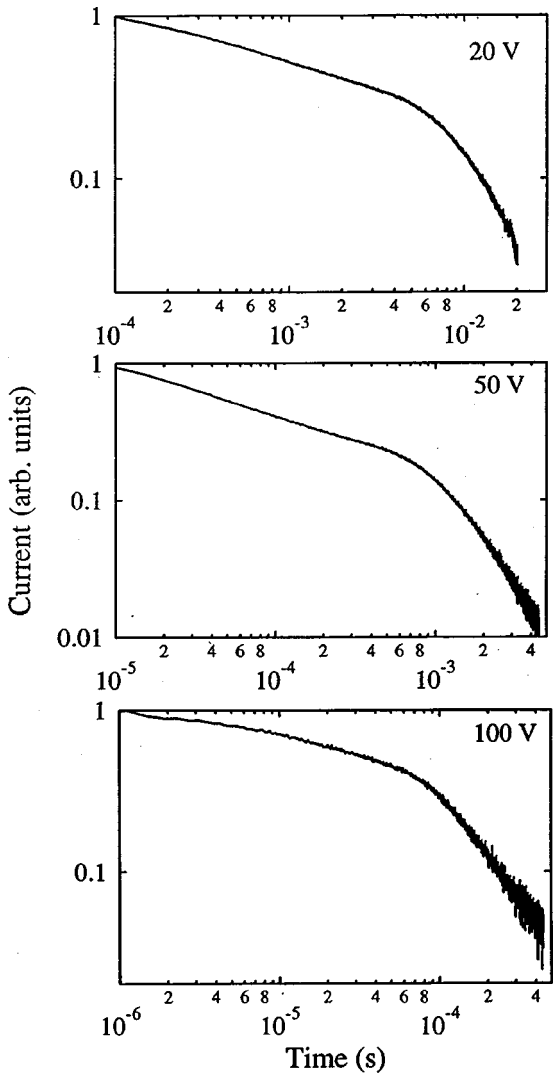

FIG. 5. Time-of-flight electron current transients at three applied voltages. The structure was Al (10 nm)/Alq (2 μm)/Al (100 nm).

$$\mu = \frac{l^2}{\tau V} \quad , \tag{7}$$

where l is the film thickness, τ is the transit time of the carriers, and V is the applied voltage. For the time-of-flight (TOF) measurements, 500-ps pulses at 370 nm from a nitrogen pumped dye laser were used as the optical excitation. The absorption coefficient of Alq at 370 nm is about 5×10^4 cm^{-1} so most of the photons are absorbed within 200 nm of the semitransparent contact.[23]

The TOF structures consisted of a thin, semitransparent Al contact on a glass substrate, an Alq layer about 2 μm thick, and a top, thick Al contact. Figure 5 is a log-log plot of the electron current as a function of time after optical excitation for applied biases of 20 V, 50 V, and 100 V. The transit time was determined by the intersection of the asymptotes to the plateau and declining slope of the current transient. The bandwidth of the current preamplifier was typically two orders of magnitude greater than the reciprocal of the transit time. The product of the structure capacitance and amplifier input impedance was at least two orders of magnitude smaller than the transit time. The total charge injected into the film was about 0.01 CV in all cases, where C is the capacitance of the structure and V the applied voltage.

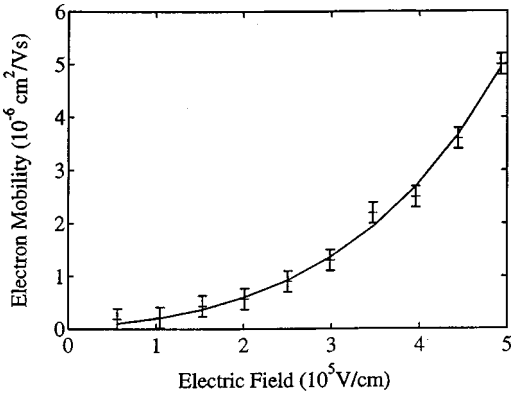

FIG. 6. Electron mobility as a function of electric field derived from the TOF measurements of Fig. 5. The markers are TOF results and the solid line is a least-squares fit to Eq. (7).

Figure 6 shows the electron mobility as a function of electric field determined from the TOF measurements (markers) and a least-squares fit (solid line) to the mobility assuming a Poole-Frenkel form

$$\mu = \mu_o \exp \sqrt{\frac{E}{E_o}} \quad , \tag{8}$$

where E is the electric field and μ_o and E_o are parameters describing the mobility. This form for the electric-field dependent mobility is frequently observed in organic molecular solids and polymers. As seen from Fig. 6, the Poole-Frenkel form accurately describes the measured TOF results. The fit to the TOF data yielded $\mu_o = 1.5 \times 10^{-8}$ cm^2/Vs and $E_o = 1.5 \times 10^4$ V/cm. It was not possible to measure the hole mobility using the TOF technique. Significant hole trapping that obscures the current transients is widely observed in Alq films.

To calculate the mobility of carriers in the solid state a quantitative understanding of the transport process is required. Recent theoretical work on spatially correlated disorder models has provided a solid starting point for determining the electric-field dependence of the solid-state mobilities.[24,25] For Alq, the correlated disorder arises from the interaction of the charge carrier with the randomly oriented dipole moments of the molecules. The mobility in the solid state is dominated by hopping between the molecules whose site energy distribution is dominated by the randomly oriented dipole moments of the individual molecules. The site energy distribution in this model has been shown to be approximately Gaussian with a standard deviation of

$$\sigma = \frac{2.35de}{\epsilon a^2}, \tag{9}$$

where a is the intermolecular spacing.[26] Using the calculated dipole moment of 5.3 D and a molecular spacing of 0.99 nm, the standard deviation is 126 meV. Because of this large width the dipole contribution to the site energy distribution most likely dominates other contributions to the energy distribution. In this model, the field dependence mobility pa-

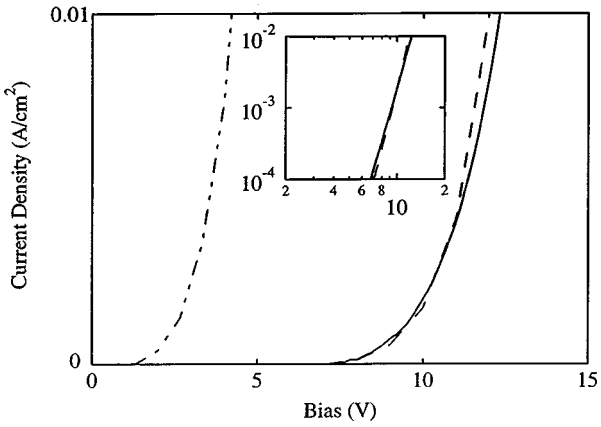

FIG. 7. Measured (solid) and calculated (dashed, dot dashed) current-voltage characteristics for Ca (20 nm)/Alq (100 nm)/Ca (100 nm) structure. The dashed (dot dashed) line is for an energy barrier of 0.62 eV (0.1 eV). The calculations used the fit to the TOF mobility shown in Fig. 6. The inset shows the measured and calculated (0.62 eV barrier) characteristics on a log-log scale.

rameter is estimated to be $E_o = 2.7 \times 10^4$ V/cm,[25] in approximate agreement with the experimental result ($E_o = 1.5 \times 10^4$) presented above.

Measurements of device current-voltage characteristics[2] suggest that the intrinsic electron and hole mobilities in Alq are comparable both in absolute value and in the strength of the field dependence. The DFT calculations support this conclusion since the computed electron and hole charged excited states have similar spatial extent and vibronic relaxation energies. If the field dependence is due to energetic disorder resulting from the charged carrier interacting with randomly arrayed molecular dipoles, it will be the same for electrons and holes. The calculated molecular properties suggest that the previously reported two order of magnitude difference between the electron and hole mobility is due to extrinsic trapping effects.[27]

In organic electronic device applications it is desirable to be able to use solid-state properties, determined from molecular calculations, to describe the measured characteristics of the organic devices. The current-voltage characteristics of electron only Alq devices were measured and compared to model calculations using the independently determined mobility and energy barrier. The *I-V* characteristics were calculated using a previously established device model that accurately describes the energy barrier dependence of conjugated polymer *I-V* characteristics.[28] Figure 7 shows measured (solid) and calculated (dashed) current-voltage characteristics for a Ca/Alq/Ca structure. The Alq layer was 100 nm thick as measured by profilometry. There is good agreement between the measured and calculated *I-V* characteristics. For the Ca contact, an energy barrier of 0.62 eV was used to describe the measured *I-V* characteristic. This energy barrier is in good agreement with the internal photoemission and built-in potential measurements discussed above. Also shown in Fig. 7 is the calculated *I-V* characteristic assuming that the contact has a 0.1 eV energy barrier (dot dash). This small energy barrier leads to space charge limited current in the Alq film and a substantially higher current-density for a given voltage.

IV. SUMMARY AND CONCLUSIONS

We used a hybrid density-functional-theory approach to calculate ground-state electronic properties and a time-dependent density-functional-theory approach to investigate the excited-state electronic properties of molecular Alq. The calculated molecular results were compared with measurements on dense solid-state films of Alq. We specifically considered: the optical absorption spectrum near the fundamental absorption threshold, the ionization potential, the single-particle energy gap, the static dielectric constant, and the electric-field dependence of the electron mobility. We found that the molecular calculations can describe the optical absorption spectrum near the fundamental absorption threshold without significant corrections for solid-state effects. The energies of the triplet states were computed and the lowest triplet lies 0.64 eV below the lowest excited singlet state. Solid-state polarization corrections are much less important for the neutral excited states that appear in optical property calculations because the response of the environment to a local dipole is much less than that for a charge. In contrast, large dielectric corrections must be included for the molecular calculations to describe the ionization potential and single-particle energy gap. When these dielectric corrections are made, using the calculated molecular polarizability, which accurately gives the measured static dielectric constant, both the ionization potential and single-particle energy gap are well described. The polarization stabilizes both the positive ion, thereby decreasing the ionization potential of the solid, and the negative ion, thereby increasing the electron affinity, relative to what would be measured or computed for the isolated molecule. The calculated molecular dipole moment can be used to interpret the electric-field dependence of the electron mobility. The solid-state properties, determined from the molecular calculations, were then used in a device model to describe the measured current-voltage characteristics in Alq diodes.

ACKNOWLEDGMENTS

The authors acknowledge financial support from the LDRD program at Los Alamos National Laboratory and thank D. R. Brown for technical assistance.

[1] C. W. Tang and S. A. Van Slyke, Appl. Phys. Lett. **51**, 913 (1987); C. W. Tang, S. A. Van Slyke, and C. H. Chen, J. Appl. Phys. **65**, 3610 (1989).

[2] I. H. Campbell and D. L. Smith, Appl. Phys. Lett. **74**, 562 (1999).

[3] W. P. Anderson, W. D. Edwards, and M. C. Zerner, Inorg. Chem. **25**, 2728 (1986); W. P. Anderson, T. R. Cundari, R. S. Drago, and M. C. Zerner, *ibid.* **29**, 1 (1990); M. Kotzian, N. Rosch, H. Schroeder, and M. C. Zerner, J. Am. Chem. Soc. **111**, 7687 (1989).

[4] P. E. Burrows, Z. Shen, V. Bulovic, D. M. McCarty, S. R. For-

rest, J. A. Cronin, and M. E. Thompson, J. Appl. Phys. **79**, 7991 (1996).

[5] A. Curioni, M. Boero, and W. Andreoni, Chem. Phys. Lett. **294**, 263 (1998).

[6] A. Curioni, W. Andreoni, R. Treusch, F. J. Himpsel, E. Haskai, P. Seidler, C. Heske, S. Kakar, T. van Buuren, and L. J. Terminello, Appl. Phys. Lett. **72**, 1575 (1998).

[7] Curioni *et al.* used the BLYP GGA, where the gradient-corrected exchange functional is due to Becke, and the gradient corrected correlation functional to Lee, Yang, and Parr. A. D. Becke, Phys. Rev. A **38**, 3098 (1988); R. Colle and O. Salvetti, J. Chem. Phys. **79**, 1404 (1983); C. Lee, W. Yang, and R. G. Parr, Phys. Rev. B **37**, 785 (1988).

[8] A. D. Becke, J. Chem. Phys. **98**, 5648 (1993); A. D. Becke, in *Modern Electronic Theory, Part II*, edited by D. A. Yarkony (World Scientific, Singapore, 1995).

[9] GAUSSIAN 98, Revision A.4, M. J. Frisch, G. W. Trucks, H. B. Schlegel, G. E. Scuseria, M. A. Robb, J. R. Cheeseman, V. G. Zakrzewski, J. A. Montgomery, Jr., R. E. Stratmann, J. C. Burant, S. Dapprich, J. M. Millam, A. D. Daniels, K. N. Kudin, M. C. Strain, O. Farkas, J. Tomasi, V. Barone, M. Cossi, R. Cammi, B. Mennucci, C. Pomelli, C. Adamo, S. Clifford, J. Ochterski, G. A. Petersson, P. Y. Ayala, Q. Cui, K. Morokuma, D. K. Malick, A. D. Rabuck, K. Raghavachari, J. B. Foresman, J. Cioslowski, J. V. Ortiz, B. B. Stefanov, G. Liu, A. Liashenko, P. Piskorz, I. Komaromi, R. Gomperts, R. L. Martin, D. J. Fox, T. Keith, M. A. Al-Laham, C. Y. Peng, A. Nanayakkara, C. Gonzalez, M. Challacombe, P. M. W. Gill, B. Johnson, W. Chen, M. W. Wong, J. L. Andres, C. Gonzalez, M. Head-Gordon, E. S. Replogle, and J. A. Pople (Gaussian, Inc., Pittsburgh, PA, 1998).

[10] I. Fujii, N. Hirayama, J. Ohtani, and K. Kodama, Anal. Sci. **12**, 153 (1998).

[11] H. Schmidbaur, J. Lettenbauer, D. L. Wilkinson, G. Muller, and O. Kumberger, Z. Naturforsch. B **46**, 901 (1991).

[12] E. K. U. Gross and W. Kohn, Adv. Quantum Chem. **21**, 255 (1990).

[13] M. E. Casida, in *Recent Advances in Density Functional Methods*, Vol. 1, edited by D. P. Chong (World Scientific, Singapore, 1995).

[14] M. E. Casida, in *Recent Developments and Applications of Modern Density Functional Theory, Theoretical and Computational Chemistry*, edited by J. M. Seminario (Elsevier, Amsterdam, 1996).

[15] M. Petersilka, U. J. Grossmann, and E. K. U. Gross, Phys. Rev. Lett. **76**, 1212 (1996); M. Petersilka and E. K. U. Gross, Int. J. Quantum Chem., Symp. **30**, 181 (1996).

[16] R. Bauernschmitt and R. Ahlrichs, Chem. Phys. Lett. **256**, 454 (1996); R. Bauernschmitt, R. Ahlrichs, F. H. Hennrich, and M. M. Kappes, J. Am. Chem. Soc. **120**, 5052 (1998).

[17] R. E. Stratmann, G. E. Scuseria, and M. J. Frisch, J. Chem. Phys. **109**, 8218 (1998).

[18] R. Williams, in *Injection Phenomena*, edited by R. K. Willardson and A. C. Beer (Academic, New York, 1970), Chap. 2.

[19] Y. Hamada, T. Sano, M. Fujita, T. Fujii, Y. Nishio, and K. Shibata, Jpn. J. Appl. Phys., Part 2 **32**, L514 (1993); A. Schmidt, M. L. Anderson, and N. R. Armstrong, J. Appl. Phys. **78**, 5619 (1995); M. Probst and R. Haight, Appl. Phys. Lett. **71**, 202 (1997).

[20] E. E. Moore and D. Yaron, J. Chem. Phys. **109**, 6147 (1998).

[21] See, for example, E. A. Silinsh and V. Capek, *Organic and Molecular Crystal* (AIP, New York, 1994), p. 109 ff.

[22] H. Schmidbauer, J. Lettenbauer, D. L. Wilkinson, G. Muller, and O. Kumberger, Z. Naturforsch. B **46**, 901 (1991).

[23] D. Z. Garbuzov, V. Bulovic, P. E. Burrows, and S. R. Forrest, Chem. Phys. Lett. **249**, 433 (1996).

[24] D. H. Dunlap, P. E. Parris, and V. M. Kenkre, Phys. Rev. Lett. **77**, 542 (1996).

[25] S. V. Novikov, D. H. Dunlap, V. M. Kenkre, P. E. Parris, and A. V. Vannikov, Phys. Rev. Lett. **81**, 4472 (1998).

[26] R. H. Young, Philos. Mag. B **72**, 435 (1995).

[27] R. G. Kepler, P. M. Beeson, S. J. Jacobs, R. A. Anderson, M. B. Sinclair, V. S. Valencia, and P. A. Cahill, Appl. Phys. Lett. **66**, 3618 (1995).

[28] P. S. Davids, I. H. Campbell, and D. L. Smith, J. Appl. Phys. **83**, 3227 (1997).